ChemPubSoc Europe

DOI: 10.1002/cctc.201600882

CHEMCATCHEM Full Papers

Synthesis and Solid-State NMR Characterization of a Robust, Pyridyl-Based Immobilized Wilkinson's Type Catalyst with High Catalytic Performance

Mohamad Srour,[a] Sara Hadjiali,[a] Grit Sauer,[a] Kai Brunnengräber,[a] Hergen Breitzke,[a] Yeping Xu,[a] Heiko Weidler,[a] Hans-Heinrich Limbach,[a, b] Torsten Gutmann,*[a] and Gerd Buntkowsky*[a]

A novel strategy for the immobilization of Wilkinson's catalyst on silica nanoparticles is presented, employing pyridyl linkers as anchoring groups. The coordination binding of the catalyst to the pyridyl linker via ligand exchange of the *trans*-phosphine group is verified by 1D and 2D solid-state NMR spectroscopy. Catalytic activities are monitored by GC employing the hydrogenation of styrene as model reaction, and the leaching properties as well as the robustness of the catalyst are investigated. The resulting immobilized catalyst shows high catalytic activity, which is within a factor of three comparable to the homogeneous catalyst, and excellent stability in leaching tests. Finally, it is efficient to produce hyperpolarization in solution by employing parahydrogen-enriched hydrogen gas for hydrogenation.

Introduction

Organometallic complexes belong to the most important homogeneous catalysts. They are employed in a wide range of organic reactions, ranging from the synthesis of fine chemicals and natural products to pharmaceuticals. Nevertheless, a long-standing problem in these syntheses is the reliable separation of the organometallic catalyst from reaction mixtures and notably from the product. This separation is necessary to minimize the heavy-metal contamination of pharmaceutical products, to protect the environment and to preserve the expensive transition-metal catalysts, in particular, in large-scale industrial processes.[1] To circumvent this problem, the immobilization of homogeneous catalysts through coordination bonds to functional groups on the surface of solid supports was suggested, a strategy that combines the advantages of homogeneous catalysts, that is, high selectivity and activity with the easy separability and recyclability of heterogeneous catalysts.[2] However, the stability of coordination bonds strongly influences the efficiency of the immobilization process and the leaching properties of the heterogenized catalysts.[3] Accordingly, many immobilized catalysts suffer from stability problems, leading to leaching of the catalytically active metals into solution and deactivation of the catalyst.[4] Thus the quest is out to develop immobilization schemes with more stable ligand coordination to prevent or at least minimize leaching.

Wilkinson's catalyst [$RhCl(PPh_3)_3$] is one of the most famous homogeneous catalysts. It was applied as an efficient catalyst for hydrogenation of alkenes, hydroformylation, hydrosilylation, and isomerization reactions.[5] Moreover, [$RhCl(PPh_3)_3$] and its derivatives were employed recently in hydrogenation reactions utilizing parahydrogen-enriched hydrogen gas for parahydrogen induced polarization (PHIP) experiments. Such PHIP experiments have high application potential in enhancing the sensitivity of NMR and magnetic resonance imaging (MRI)[6] techniques, for example, in biomedicine.[7] Furthermore, PHIP was employed in mechanistic studies to monitor reaction intermediates and even low amounts of product molecules formed during reactions.[8]

This wide applicability has driven various attempts to immobilize the homogeneous Wilkinson's catalyst or analoga on solid support materials.[9] Most of these works are related to the formation of coordination bonds between the rhodium metallic center of Wilkinson's catalyst and suitable functional groups, which were grafted on the surface of solid supports such as silica nanoparticles or polystyrene. Mainly linker molecules containing phosphine groups or aliphatic amines were employed, which form Rh–P[9a–g,10] or Rh–N[9g–i] coordination bonds, respectively.

As typical examples for phosphine-containing linkers, the Rh–P type immobilized Wilkinson's catalysts [Rh–P–Wilk] have shown significant catalytic activity in hydrogenation reactions and good separability.[9b,c] However, a gradual loss of the

[a] M. Srour, S. Hadjiali, Dr. G. Sauer, K. Brunnengräber, Dr. H. Breitzke, Dr. Y. Xu, H. Weidler, Prof.Dr. H.-H. Limbach, Dr. T. Gutmann, G. Buntkowsky
Institute of Physical Chemistry
Technical University Darmstadt
Alarich-Weiss-Straße 8, 64287 Darmstadt (Germany)
E-mail: gutmann@chemie.tu-darmstadt.de
gerd.buntkowsky@chemie.tu-darmstadt.de

[b] Prof.Dr. H.-H. Limbach
Institute of Chemistry and Biochemistry
Freie Universität Berlin
Takustraße 3, 17195 Berlin (Germany)

Supporting information and the ORCID identification number(s) for the author(s) of this article can be found under http://dx.doi.org/10.1002/cctc.201600882.

catalytic activity was observed, mainly caused by the leaching of catalytic active species from the surface, as shown by (PHIP) NMR experiments.[9f] Furthermore, as phosphine linker groups and ligands are easily oxidized in solution, they become unable to re-coordinate the rhodium metallic center and the catalytic activity decreases.[9a–c] For amine linkers, the Rh–N type immobilized Wilkinson's catalyst [Rh–N–Wilk] was employed in the hydroformylation of cyclohexane by Huang et al., who obtained efficient catalytic activity, however, with a relatively high loss of rhodium content.[9j] Moreover, Rh–N type immobilized Wilkinson's type catalysts were employed in the hydrogenation of triple bonds at room temperature as efficient catalysts showing nonsignificant leaching.[11] This led us assume that the relatively large loss of Rh in the work of Huang et al. was a consequence of elevated temperature conditions.

Thus, it is necessary to employ linkers with alternative functional groups that offer both, high stability at elevated temperature and preservation of high catalytic performance of the Wilkinson's catalyst. From the work by Heaton et al.[12] it is known that pyridine can replace one or more phosphine groups of the homogeneous Wilkinson's catalyst and coordinate to Rh after ligand exchange reaction. Such homogeneous complexes were found as efficient catalysts for reductive coupling of aldehydes and hydrogenation reactions, despite the fact that pyridyl groups are usually more labile than phosphine ligands. However, in contrast to phosphine, pyridine is not prone to oxidation. Further examples for highly efficient pyridine-based homogeneous catalysts are known for ruthenium which has been employed for olefin and cross metathesis reactions.[13]

Based on these results obtained for homogeneous catalysts, we decided to study the immobilization of Wilkinson's catalyst on a solid support containing linkers with pyridyl functional groups and synthesized a Rh–[Py] type catalyst. Silica nanoparticles [SiO_2] were chosen as carrier material, to prepare pyridyl-functionalized silica materials [SiO_2–Py]. Additionally, we wanted to investigate whether the pyridyl groups of the linker can replace one or more of the phosphine groups of the Wilkinson's catalyst [$RhCl(PPh_3)_3$] through a ligand exchange reaction and coordinate to the rhodium by forming Rh–[Py] bonds to obtain a novel immobilized catalyst of the type [SiO_2–Py–Wilk].

Firstly the synthesis and basic characterization of the novel [SiO_2–Py–Wilk] catalyst is described. The synthesis steps are then investigated by employing a combination of multinuclear (^{29}Si, ^{13}C, and ^{31}P) solid-state NMR spectroscopy and 2D ^{1}H–^{31}P heteronuclear correlation (HETCOR) NMR experiments. Then, the catalytic activity of the new immobilized catalyst [SiO_2–Py–Wilk] is studied for the hydrogenation reaction of styrene and compared to the catalytic activity of the homogeneous [$RhCl(PPh_3)_3$] catalyst. Next, the applicability of this new catalyst for PHIP experiments is investigated and compared to the [Rh–P–Wilk] catalyst. Finally, the stability and leaching properties of the [SiO_2–Py–Wilk] catalyst are evaluated.

Results and Discussion

Synthesis of the immobilized catalyst [SiO_2–Py–Wilk] and its basic characterization

In the first step of the synthesis (Scheme 1), the silica nanoparticles [SiO_2] were dried under vacuum at 423 K to remove adsorbed water molecules, and activate the terminal Si–OH groups. Then, the pyridyl linker was grafted on the surface according to literature procedures[9h,14] to form the functionalized silica support material [SiO_2–Py]. By elemental analysis (see the Supporting Information, Table S1) the grafting density (GD) of the linker on the silica surface was approximated at approximately 2×10^{-6} mol m^{-2}, by following the procedure described in the Supporting Information.

In the next step, the [$RhCl(PPh_3)_3$] catalyst in toluene was added to the functionalized silica [SiO_2–Py] and stirred under reflux conditions to produce the immobilized catalyst [SiO_2–Py–Wilk]. The analysis of the rhodium content of the product was performed by inductively coupled plasma optical emission spectroscopy (ICP–OES), which yielded a value of approximately 1 wt% Rh. This clearly indicates the presence of rhodium catalyst after immobilization.

Characterization by ^{13}C and ^{29}Si cross-polarization magic-angle spinning NMR spectroscopy

Elemental analysis cannot confirm whether the linkers are covalently bound to the silica surface, and whether the rhodium is coordinated by pyridyl groups of the linker after a ligand exchange of the phosphine with the pyridyl. To answer these

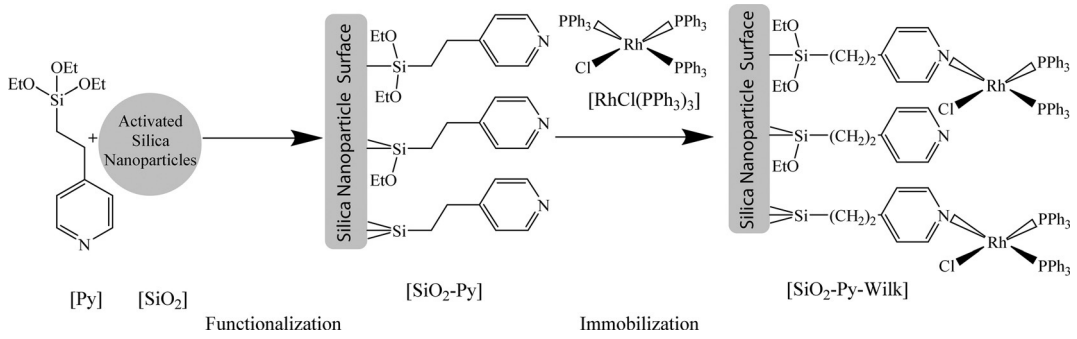

Scheme 1. Functionalization of [SiO_2] and immobilization of [$RhCl(PPh_3)_3$] to produce the immobilized catalyst [SiO_2–Py–Wilk].

questions, solid-state NMR techniques were employed. In a first step, the ^{29}Si cross-polarization magic-angle spinning (CP–MAS) NMR spectra of nonfunctionalized silica [SiO_2] and the functionalized silica [SiO_2–Py] were recorded (see the Supporting Information, Figure S1). The broad peak visible between −94 and −115 ppm was found in both ^{29}Si spectra. It is characteristic for silicon atoms of the Q_n groups in bulk silica material. The peaks visible between −48 and −67 ppm, which appear only in the spectrum of the functionalized silica (Figure S1 b), have the typical chemical shift values of T_n groups, which are characteristic for the binding of an alkoxy- or alkyl containing linker to the silica surface (see refs. [9a, g, h]). These results clearly demonstrate that the pyridine linkers are covalently bound to the silica nanoparticles [SiO_2] surface and the successful synthesis of [SiO_2–Py].

To corroborate the success of the functionalization step, the ^{13}C CP–MAS NMR spectrum of [SiO_2–Py] (Figure 1 a) and the liquid ^{13}C NMR spectrum of the pyridine linker [Py] (see Figure 1 b) were compared. The detected signals of the functionalized silica are broadened compared to the signals of the free pyridine linker [Py], which is a clear indication that after functionalization the pyridine linker is present in a disordered environment.

After reaction of the Wilkinson's catalyst with the functionalized silica material, the ^{29}Si and ^{13}C CP–MAS NMR spectra of the heterogeneous catalyst [SiO_2–Py–Wilk] were acquired. Whereas the ^{29}Si spectrum (not shown) did not change after addition of the homogeneous catalyst, a new peak appeared at approximately 128 ppm as shoulder in the ^{13}C NMR spectrum (Figure 1 a), which is assigned to the aromatic carbon atoms of the PPh_3 groups, which are typically found in the aromatic region at approximately 128–130 ppm. Nevertheless, as this region is heavily cluttered by the signal of the pyridyl groups, the final prove of the coordination binding of the catalyst requires solid-state ^{31}P NMR spectroscopy, which is a more efficient probe for the characterization of phosphine-containing catalysts.[9a, g, h, 20]

Characterization by 1 D and 2 D ^{31}P solid-state NMR techniques

In Figure 2, the ^{31}P CP–MAS NMR spectrum of the immobilized catalyst [SiO_2–Py–Wilk] is displayed. Three sets of signals at 55.8, 48.6, and approximately 28.7 ppm are distinguished in the spectrum. The broad upfield peak at 28.7 ppm is assigned to physisorbed and chemisorbed triphenylphosphine oxide ($OPPh_3$) according to the literature[21] which is formed by oxidation of the leaving PPh_3 group during the immobilization step.

The chemical shifts of the two downfield sets of signals at 55.8 and 48.6 ppm are comparable with the chemical shifts

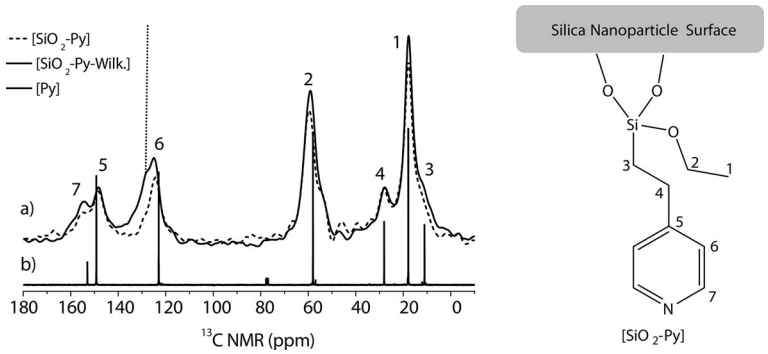

Figure 1. (a) ^{13}C CP–MAS NMR spectra measured at 10 kHz spinning of the functionalized silica [SiO_2–Py] (dashed line) and the immobilized catalyst [SiO_2–Py–Wilk] (solid line). (b) ^{13}C solution NMR spectrum of the pyridine linker [Py]. The schematic structure of the functionalized silica is given on the right.

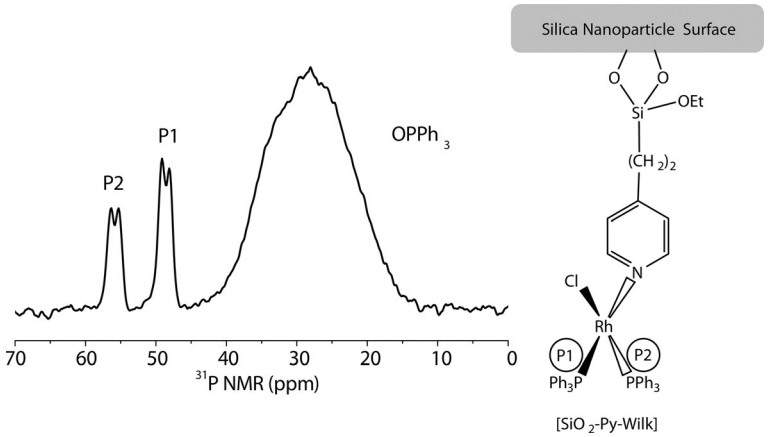

Figure 2. ^{31}P CP–MAS spectrum of [SiO_2–Py–Wilk] measured at 10 kHz spinning.

that were observed by Heaton et al. in the ^{31}P NMR spectrum of *cis*-[RhCl(py)(PPh_3)$_2$] (at 54.3 and 49 ppm).[12] This indicates that in our work the pyridyl moiety on the surface of the functionalized silica [SiO_2–Py] reacts with Wilkinson's catalyst similarly to the pyridyl moieties in Heaton's work. We assume that the phosphine ligand, located in *cis* position with respect to chloride atom in [RhCl(PPh_3)$_3$] is exchanged by a pyridyl ligand from the surface of [SiO_2–Py], referring to the work of Goodman et al.,[22] who showed that PPh_3 groups in *cis* position to chloride in Wilkinson's catalyst are faster released than PPh_3 groups in *trans* position to chloride. The remaining two phosphine groups are thus attributed to the lines at 48.6 ppm (P1) and 55.8 ppm (P2) by virtue of the weaker Rh–P2 π back-bonding effect of P2.

If the pyridyl linker behaves similar to the pyridine in solution, one can further expect that the remaining two phosphine groups (P1 and P2) are still coordinated to the Rh and aligned in *cis* configuration with respect to each other. To probe the latter, it is necessary to look at the ^{31}P homonuclear scalar couplings of the immobilized complex. The signals assigned to P1 and P2 are split into doublets as a consequence of the ^1J(Rh–P) coupling, which measures 186 Hz for P1 and 191 Hz for P2. In the case of a *trans* configuration a strong $^2J(^{31}P1–^{31}P2)$ coupling of ca. 400 Hz and in the case of a *cis* configuration a very weak $^2J(^{31}P1–^{31}P2)$ coupling in the range of 0 and 50 Hz is expected.[20b]

In principle, there are two different binding scenarios that can explain the observed spectra and the absence of a strong $^2J(^{31}P1–^{31}P2)$ coupling. In the first scenario a single pyridyl linker replaces one of the *trans*-phosphine ligands, leading to a bound catalyst with two remaining *cis*-phosphine ligands. In the second scenario, two pyridyl linkers replace two phosphine groups and the two different chemical shifts are the results of the *cis*-pyridyl and *trans*-pyridyl-configuration. Although in principle a ^{31}P–^{31}P double quantum NMR experiment[23] could decide between these scenarios, the signal losses in the excitation, evolution, and reconversion phases of the DQ experiment plus the presence of spurious ^{31}P–^{31}P dipolar interactions to neighboring free phosphine groups render this approach futile.

The 2D ^{1}H–^{31}P HETCOR spectrum (Figure 3) illustrates that both ^{31}P peaks at 55.8 and 48.6 ppm in f2 correlate to aliphatic protons at approximately 3–4 ppm, which belong to the alkyl chains of the pyridine linkers [Py]. In addition, these ^{31}P peaks correlate to two sets of aromatic protons, the first aromatic set of which visible at approximately 7–8 ppm assigns to the protons of the phenyl ring in the phosphine groups and to the proton in *meta* position of the pyridyl moiety in [SiO_2–Py], and the second aromatic set at approximately 9–10 ppm belongs to the *ortho* protons in the pyridyl moiety in [SiO_2–Py]. Furthermore, in the 2D ^{1}H–^{31}P HETCOR spectrum, the broad ^{31}P peak at 28.7 ppm in f2 shows three correlation peaks to protons in f1. One correlation peak is observed in the Si–OH proton region of the f1 scale at approximately 1–2 ppm and another one reveals in the aliphatic region at approximately 3–4 ppm. Those peaks reflect magnetization transfer from the protons of the silica surface and the aliphatic part of the [Py] linker

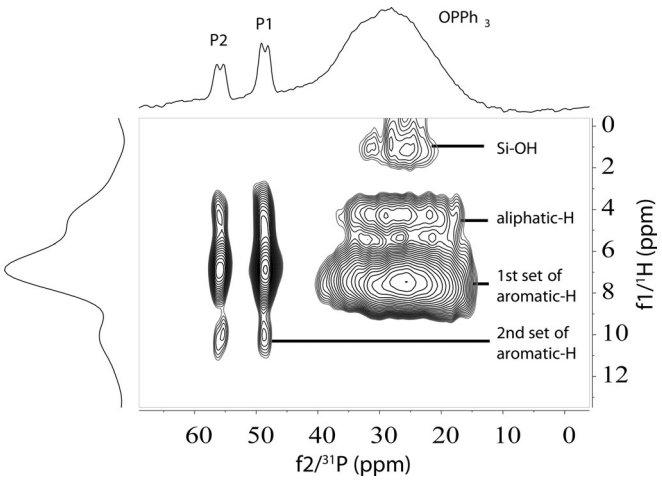

Figure 3. 2D ^{1}H–^{31}P HETCOR spectrum measured at 10 kHz spinning of [SiO_2–Py–Wilk]. The f1 and f2 scales refer to ^{1}H and ^{31}P chemical shifts scales, respectively.

respectively, to the neighboring adsorbed $OPPh_3$ on the surface of silica. Finally, a third correlation peak is found in the aromatic region of the f1 scale at approximately 7–8 ppm and consequently is assigned to the phenyl group of $OPPh_3$.

The presence of correlation peaks between the ^{1}H of the pyridyl moiety bound to the silica surface and ^{31}P of the two phosphine groups clearly evidence the close spatial proximity between the pyridyl moiety and the two phosphine groups. Moreover, one can notice that these correlation peaks have lower intensity than the correlation peak between ^{1}H and ^{31}P of the two phosphine groups. This shows that these protons have a larger distance from the phosphine groups than the protons of the phenyl groups of the PPh_3, which clearly evidences the formation of a coordination bond from the pyridyl to the rhodium center.

Thus, by combining the results from the solid-state NMR experiments, we can conclude that the interaction of the Wilkinson's catalyst with the pyridyl linker is comparable with the interaction of the Wilkinson's catalyst with neat pyridine, namely the replacement of the *trans*-phosphine group and the formation of a coordination bond to the ring nitrogen.

Catalytic hydrogenation

In Table 1 the results from the catalytic tests of the immobilized Wilkinson's catalyst [SiO_2–Py–Wilk] are collected for equimolar concentrations of active rhodium sites. At 5 bar and 75 °C the time factor of only three is obtained between the homogeneous catalyst [RhCl(PPh_3)$_3$] and the new immobilized [SiO_2–Py–Wilk] for full conversion of styrene into ethylbenzene (1 and 3 h, respectively). Similar results are obtained at 105 °C.

This high efficiency is also represented by the turnover numbers (TON) of the catalyst in the reactions (Figure 4), in which TON is the number of substrate (styrene) molecules converted to ethylbenzene at defined time per catalyst molecule. The number of catalyst molecules of [SiO_2–Py–Wilk] was calculated from ICP–OES results under the assumption that all rhodium

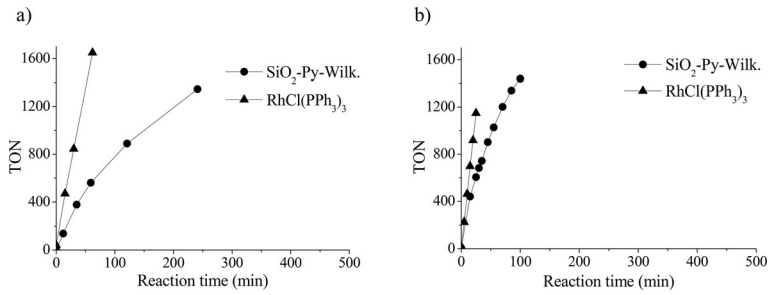

Figure 4. Evolving TON of styrene vs. time at two reaction temperatures at 5 bar hydrogen pressure catalyzed by [SiO_2–Py–Wilk] (●) and [$RhCl(PPh_3)_3$] (▲) at a) 75 °C and b) 105 °C.

Table 1. Catalytic activity tests of [SiO_2–Py–Wilk] and [$RhCl(PPh_3)_3$] catalysts at different reaction conditions.

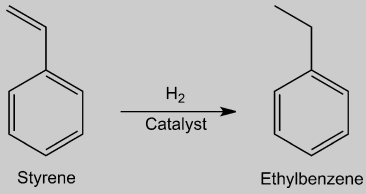

Catalyst	Conversion [%]	*t* [min]	Reaction conditions
[SiO_2–Py–Wilk]	94.3	241	5 bar/75 °C
[$RhCl(PPh_3)_3$]	93.7	62	
[SiO_2–Py–Wilk]	96.9	100	5 bar/105 °C
[$RhCl(PPh_3)_3$]	99.9	30	

sites are accessible by the substrate. The activity tests in Figure 4 clearly demonstrate that both [$RhCl(PPh_3)_3$] and [SiO_2–Py–Wilk] catalysts initially obey the characteristic zero-order rate with the linear relation between reaction time and TON. Upon the increase in reaction time there is a change towards a higher reaction order of [SiO_2–Py–Wilk], visible as the curvature in the graph. This curvature is most probably the result of transport processes, in particular, the diffusion of substrate molecules to the surface becomes the rate-limiting factor for the heterogeneous [SiO_2–Py–Wilk].

Leaching study of [SiO_2–Py–Wilk]

By performing the hydrogenation reaction of the filtrate solutions after removing the heterogeneous catalyst, no catalytic activity was detected by GC. Although most other hydrogenations were performed at mild conditions of 1 bar and 75 °C, the leaching test was performed at the more harsh conditions of 5 bar and 105 °C to enforce possible leaching effects. This clearly shows that the heterogeneous [SiO_2–Py–Wilk] catalyst is the catalytic active species, and there are no significant amounts of leached catalytic centers inside the filtrate. More importantly, ICP–OES of the filtrates confirms that rhodium amounts of less than 1 ppm are present in the filtrate. This result gives strong evidence of the robustness of the Rh–Py bond within the [SiO_2–Py–Wilk] catalyst, which renders the pyridyl group as highly efficient immobilizing group.

Reusability tests of [SiO_2–Py–Wilk]

In the next step we studied the reusability of the [SiO_2–Py–Wilk] catalyst. As shown in Figure 5 there is a strong increase of the catalytic activity in the course of the reaction/recovery cycles, leading to approximately a doubling of TON after three cycles compared to one cycle.

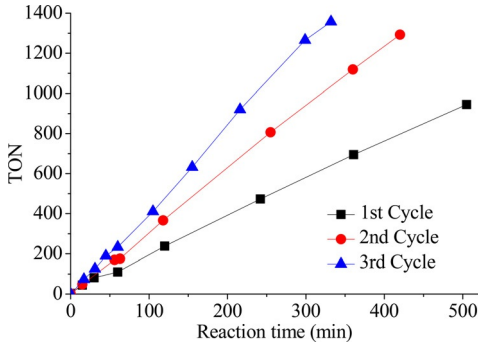

Figure 5. TON of styrene vs. time of hydrogenation reaction performed at 1 bar and 75 °C catalyzed by the immobilized catalyst [SiO_2–Py–Wilk] for three successive cycles.

These experiments indicate that the catalytic activity of [SiO_2–Py–Wilk] catalyst requires an activation step. To get insight into this activation step, we measured the ^{31}P CP–MAS NMR spectra of the dried catalyst after the cycles and the ^{31}P solution NMR spectrum of the filtrate after the first cycle of the reusability test (Figure S3). The solution NMR spectrum revealed the presence of dissolved free phosphine groups and phosphine oxide at shift of −6 ppm (PPh_3) and 23.5 ppm ($OPPh_3$) respectively, and the CP–MAS spectra showed the disappearance of the resolved ^{31}P signals at 55.8 and 48.6 ppm and a broadening of the signal of phosphine oxides. These results indicate that the first step of the activation of the catalyst is mainly the replacement of PPh_3 groups from the pristine catalyst. They leave into solution and are later oxidized.

Interestingly, the spectra of the filtrate after two and three cycles do no longer show any significant signals of phosphine or phosphine oxide, despite the fact that the catalytic activity is growing. This finding indicates that a second activation step is responsible for the final high activity. A possible process could be the reduction of the rhodium and the formation

of small catalytically active Rh clusters or nanoparticles on the silica surface. Such a process was reported recently by Koptyug and co-workers,[6e,24] during gas phase hydrogenation processes.

PHIP experiment

Finally we were interested whether our catalyst is suitable for PHIP experiments (Figure 6). Before performing PHIP experiments, the spectrum of the reaction mixture was recorded (Figure 6a) which is employed as a thermal reference spectrum. Here only the signals of styrene between $\delta = 5.0$ and

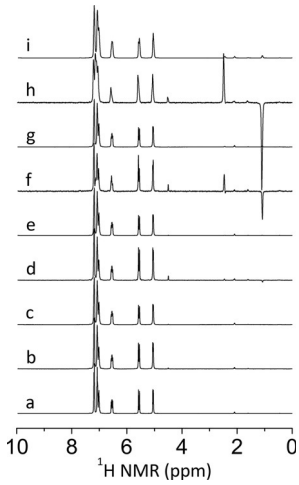

Figure 6. ^{1}H NMR spectra of the styrene hydrogenation in [D_8]toluene employing [SiO_2–Py–Wilk] as a catalyst: a) reaction mixture before hydrogenation, b, d, f, h) single-scan spectra after hydrogenation with parahydrogen-enriched hydrogen PHIP1–4, respectively; c, e, g, i) four-scan spectra recorded after relaxation of the hyperpolarized spin state of PHIP1–4, respectively. Note: The signals of styrene are located between 5.0 and 7.3 ppm. The signal at 2.1 ppm belongs to residual hydrogen atoms in the methyl group of [D_8]toluene. The signal of dissolved orthohydrogen is visible at 4.6 ppm. The signals of ethylbenzene are located at 1.1 ppm (CH_3) and 2.5 ppm (CH_2). Spectra were normalized to the toluene signal at 2.1 ppm.

7.3 ppm and a signal at 2.1 ppm belonging to residual hydrogen atoms in the methyl group of [D_8]toluene are visible. For each experiment, PHIP spectra were measured to detect the hyperpolarized spin state of the product (ethylbenzene, displayed in Figure 6b, d, f, and h), and for comparison the thermal spectra were recorded after relaxation of the hyperpolarized spin state (illustrated in Figure 6c, e, g, and i). Each spectrum recorded after relaxation is employed as thermal reference spectrum for the following PHIP experiment.

The PHIP experiments corroborate the finding that the catalysts need an initial activation step. Whereas after the first hydrogenation (PHIP 1) no PHIP activity of [SiO_2–Py–Wilk] was visible, slight activity in the hydrogenation with parahydrogen was observed after the second hydrogenation step (PHIP 2), and finally a much higher activity was observed in the third and the fourth step (PHIP 3 and PHIP 4).

To calculate the signal enhancement (SE) obtained for each PHIP experiment, the PHIP signals were integrated and compared to the thermal signals of the product in the relaxed spectrum according to Equation (E3) in the Supporting Information. For PHIP 3 and PHIP 4 respectively, signal enhancements of approximately 38 and 57 were obtained for the CH_3 group, and of approximately 36 and 51 for the CH_2 group.

To confirm that the hyperpolarization was produced by the heterogeneous catalyst [SiO_2–Py–Wilk], the solid catalyst was removed from the reaction mixture and three subsequent PHIP experiments were performed on the filtrate solution. No increase in the product signals was observed in the relaxed spectra after the filtrate was hydrogenated with parahydrogen (see Figure S4). Therefore, it is strongly supposed that the hyperpolarization is produced by the activated heterogeneous catalyst.

Finally, we note that the observed PHIP enhancements were only moderate, however, a scale-up of the PHIP activity is feasible by employing a reaction chamber with higher catalyst concentrations.

Conclusions

A novel strategy for the immobilization of the well-known Wilkinson's catalyst on silica nanoparticles employing pyridyl linkers is presented. The coordination binding of the catalyst to the pyridyl linker through ligand exchange of the *trans*-phosphine group is proven by solid-state NMR techniques.

The resulting immobilized catalyst [SiO_2–Py–Wilk] shows excellent catalytic activity, which is within a factor of three comparable to the homogeneous catalyst, and excellent stability in leaching tests. Moreover, this catalyst produces acceptable activity in the hydrogenation with parahydrogen with significant signal enhancement for the hydrogenation of styrene. This observation qualifies this heterogenized catalyst to be developed as prospective tool for sensitivity enhancement in NMR and magnetic resonance imaging applications. Thus, in summary one can conclude that pyridyl linkers can be employed as efficient alternative to phosphine and amine linkers in the immobilization of Wilkinson's and related homogeneous catalysts.

Experimental Section

Materials

Chemicals were purchased and used without further purifications as follows, [SiO_2] from Sigma–Aldrich, the pyridine linker 2-(4-pyridylethyl) triethoxysilane [Py] and [$RhCl(PPh_3)_3$] from ABCR GmbH&Co. KG, and styrene from Merck KGaA. Toluene and dichloroethane were dried under an argon atmosphere employing standard procedures. All reactions were performed under argon using Schlenk technique.

Preparation of the immobilized Wilkinson's catalysts [SiO_2–Py–Wilk]

In a first step, silica nanoparticles [SiO_2] were activated by drying them for 14 h under vacuum at 423 K. The activated silica was then functionalized according to the procedure described in refs. [9h, 14]. Typically, the activated silica (2 g) was heated at reflux with the linker (2 g) in dry toluene (50 mL) for 3 h. The resulting

suspension was filtrated and washed with dichloromethane employing Soxhlet extraction. The final product was dried overnight under vacuum yielding the functionalized silica [SiO_2–Py] as a powder. Next, [SiO_2-Py] (2 g) and the homogeneous Wilkinson's catalyst [$RhCl(PPh_3)_3$] (0.2 g) were placed in a two-necked flask which was then evacuated for 30 min. The flask was then set under argon and dry toluene (50 mL) was added. Afterwards, the mixture was heated at reflux for 3 h to perform the immobilization reaction. The immobilized catalyst [SiO_2–Py–Wilk] was filtrated from the suspension, washed with dry toluene using Soxhlet extraction, dried overnight, and kept in a glovebox.

Elemental analysis

The approximate grafting density of the linker [Py] on the surface of the functionalized silica nanoparticles [SiO_2-Py] was determined according to the procedure described by Pardal et al.[15] by elemental analysis, employing a VarioEL III elemental analysis system in CHN mode (for details of the calculation see ESI).

The rhodium content in [SiO_2–Py–Wilk] was detected by ICP–OES. Experiments were performed by the CURRENTA GmbH. Microwave-assisted digestion the immobilized catalyst (0.6 g) was performed on a mixture of nitric and hydrofluoric acid prior to the detection of the rhodium content in the sample by means of ICP–OES.

Solid-state NMR experiments

All solid-state NMR experiments were performed on a Bruker AVANCE II + spectrometer at 400 MHz proton resonance frequency, employing a Bruker 4 mm double resonance probe at room temperature.

Spectra were recorded utilizing ramped CP–MAS sequences, at spinning rates of 5 kHz for ^{29}Si and 10 kHz for ^{13}C and ^{31}P. Contact times were set to 6.5 ms for ^{29}Si CP–MAS experiments, 1 ms for ^{13}C CP–MAS experiments and 2 ms for ^{31}P CP experiments. ^{31}P–^{1}H HETCOR spectra were acquired with 2 ms contact time. FSLG homonuclear decoupling was utilized with a decoupling field of 71 kHz during the evolution of the chemical shift.[16] Tppm20 decoupling[17] was applied for all experiments during data acquisition. ^{29}Si and ^{13}C spectra were referenced with respect to tetramethylsilane, ^{1}H signal was set internally to the aromatic peak at 7 ppm and ^{31}P spectra were calibrated utilizing H_3PO_4 (0 ppm) as external standard.

Catalytic hydrogenation

The hydrogenation tests were performed employing a Fisher–Porter–Bottle (FPB) connected with a hydrogen gas source and a Schlenk line. The hydrogenation tests were performed at 5 bar hydrogen gas pressure at either 75 °C or 105 °C reaction temperature. A mixture of [SiO_2-Py-Wilk] (70 mg, 6.7×10^{-3} mmol calculated from the rhodium content of the sample) and dry toluene (9 mL) was placed in the FPB, degassed, and heated up to the nominated temperature (75 °C or 105 °C). The hydrogen pressure was adjusted before the beginning of the hydrogenation reaction and kept stable during the reaction. In a typical procedure, the reaction was started by injecting styrene (1 mL) as a model substrate into the catalyst suspension. The course of the reaction was monitored by taking samples at defined times (see Table S2), and analyzing them through GC. The catalytic activity of the new catalyst [SiO_2–Py–Wilk] was compared to the activity of Wilkinson's catalyst [$RhCl(PPh_3)_3$], by repeating the hydrogenation test under the same conditions, employing the homogeneous Wilkinson's catalyst [$RhCl(PPh_3)_3$] (7 mg, 7.6×10^{-3} mmol).

Leaching tests of [SiO_2–Py–Wilk]

After each catalytic activity test, the solid catalyst [SiO_2–Py–Wilk] was filtrated from the reaction mixture to investigate its leaching properties. Benzene-d_6 was added to the filtrate solution to record its ^{31}P NMR solution NMR spectrum to inspect whether there are leached phosphine species. To analyze whether catalytic active species were present in the filtrate solution, it was transferred into a FPB together with 0.5 mL of styrene to perform the catalytic test by heating the mixture up to 105 °C and applying a hydrogen pressure of 5 bar. For each leaching test, two samples were taken and measured by GC, one immediately after the addition of styrene and the second after 3 h of reaction to monitor the reaction progress. To quantify and reconfirm the leaching test results, the filtrates were collected again and digested in nitric and hydrofluoric acid to determine their rhodium content by means of ICP–OES.

PHIP experiments

The sample for PHIP experiments was prepared by transferring [SiO_2-Py-Wilk] (10 mg) styrene (0.1 mL) and [D_8]toluene (0.7 mL) of into a 5 mm screw-cap NMR sample tube. By cooling H_2 to 77 K in the presence of activated charcoal, parahydrogen was enriched with a laboratory-built apparatus described in the literature.[18] The hydrogenation with parahydrogen (PHIP1) was performed in the Earth magnetic field under ALTADENA[19] conditions employing 2 bar of para-enriched H_2 and heating the reaction mixture at the boiling point. After ≈10–15 s reaction time, the sample was transferred into the strong magnetic field of a 11.7 Tesla Bruker AVANCE III 500 spectrometer. Using 1 scan and a RF-pulse of 14 μs, a series of ^{1}H NMR spectra with a delay time of 8.5 s between two subsequent spectra were recorded until full relaxation of the hyperpolarized spin state. Finally, three subsequent hydrogenation steps with parahydrogen were performed (PHIP2, PHIP3, and PHIP4) following the same procedure as for PHIP1. Thermal spectra were recorded before each PHIP experiment and after full relaxation of the PHIP signals, respectively, employing 4 scans and a RF-pulse of 14 μs.

To confirm that the heterogeneous catalyst [SiO_2–Py–Wilk] produced the hyperpolarized spin state, the catalyst was removed from the reaction mixture by filtration using a cellulose membrane filter with a pore size of 0.2 μm. Finally, the filtrate was transferred into a 5 mm screw-cap NMR sample tube to perform hydrogenation with parahydrogen on the filtrate.

Reusability test of [SiO_2–Py–Wilk]

An exemplary reusability test of the [SiO_2-Py-Wilk] catalyst was performed at 1 bar hydrogen pressure and at 75 °C. After one cycle of the styrene hydrogenation, the [SiO_2–Py–Wilk] catalyst was filtrated from the reaction mixture and dried overnight to be used for the second cycle which was performed under the same conditions as in the first cycle. This procedure was repeated again to get the results for the third cycle. The filtrate of each cycle was kept to investigate the leaching properties according to the above described procedure.

Acknowledgements

This work has been supported by the Deutsche Forschungsgemeinschaft (DFG) under contract Bu-911-22-1. GB gratefully acknowledges financial support by the state of Hessia, LOEWE iNAPO.

Keywords: heterogeneous catalysis · hydrogenation · immobilization · phosphane ligands · rhodium

[1] a) J. Hagen in *Industrial Catalysis: A Practical Approach*, Wiley-VCH, Weinheim, **2006**, pp. 1–14; b) D. Macquarrie in *Heterogenized Homogeneous Catalysts for Fine Chemicals Production: Materials and Processes*, Springer Netherlands, Dordrecht, **2010**, pp. 1–35.

[2] a) X. S. Zhao, X. Y. Bao, W. P. Guo, F. Y. Lee, *Mater. Today* **2006**, *9*, 32–39; b) F. Cozzi, *Adv. Synth. Catal.* **2006**, *348*, 1367–1390; c) W. G. Lu, D. Q. Yuan, D. Zhao, C. I. Schilling, O. Plietzsch, T. Muller, S. Bräse, J. Guenther, J. Blümel, R. Krishna, Z. Li, H. C. Zhou, *Chem. Mater.* **2010**, *22*, 5964–5972; d) N. End, K.-U. Schöning in *Immobilized Catalysts, Vol. 242* (Ed.: A. Kirschning), Springer, Berlin, **2004**, pp. 241–271; e) C. Copéret, J. M. Basset, *Adv. Synth. Catal.* **2007**, *349*, 78–92.

[3] a) V. Polshettiwar, C. Len, A. Fihri, *Coord. Chem. Rev.* **2009**, *253*, 2599–2626; b) F. Teixeira, R. A. Mosquera, A. Melo, C. Freire, M. N. D. S. Cordeiro, *J. Phys. Chem. A* **2014**, *118*, 10788–10796; c) J. L. Huang, M. T. Wang, S. Y. Zhang, B. W. Hu, H. X. Li, *J. Phys. Chem. C* **2011**, *115*, 22514–22522.

[4] a) D. Cantillo, C. O. Kappe, *Chim. Oggi* **2015**, *33*, 6–10; b) G. J. Sherborne, M. R. Chapman, A. J. Blacker, R. A. Bourne, T. W. Chamberlain, B. D. Crossley, S. J. Lucas, P. C. McGowan, M. A. Newton, T. E. O. Screen, P. Thompson, C. E. Willans, B. N. Nguyen, *J. Am. Chem. Soc.* **2015**, *137*, 4151–4157; c) D. Cantillo, C. O. Kappe, *ChemCatChem* **2014**, *6*, 3286–3305; d) H. Gruber-Woelfler, P. F. Radaschitz, P. W. Feenstra, W. Haas, J. G. Khinast, *J. Catal.* **2012**, *286*, 30–40.

[5] a) J. A. Bae, K. C. Song, J. K. Jeon, Y. S. Ko, Y. K. Park, J. H. Yim, *Microporous Mesoporous Mater.* **2009**, *123*, 289–297; b) P. Li, W. Thitsartarn, S. Kawi, *Ind. Eng. Chem. Res.* **2009**, *48*, 1824–1830; c) F. H. Jardine, *Prog. Inorg. Chem.* **1981**, *28*, 63–202; d) M. Tuner, J. V. Jouanne, H. D. Brauer, H. Kelm, *J. Mol. Catal.* **1979**, *5*, 433–445; e) M. Tuner, J. V. Jouanne, H. D. Brauer, H. Kelm, *J. Mol. Catal.* **1979**, *5*, 425–431; f) V. Macho, F. Halmo, *Petrochemia* **1974**, *14*, 117–122; g) R. L. Augustine, J. F. van Peppen, *J. Chem. Soc. D* **1970**, 495–496; h) C. H. Heathcock, S. R. Poulter, *Tetrahedron Lett.* **1969**, *10*, 2755–2758; i) G. C. Bond, R. A. Hillyard, *Discuss. Faraday Soc.* **1968**, *46*, 20–30; j) D. Evans, J. A. Osborn, G. Wilkinson, *J. Chem. Soc. A* **1968**, 3133–3142; k) J. A. Osborn, F. H. Jardine, J. F. Young, G. Wilkinson, *J. Chem. Soc. A* **1966**, 1711–1732.

[6] a) L. S. Bouchard, K. V. Kovtunov, S. R. Burt, M. S. Anwar, I. V. Koptyug, R. Z. Sagdeev, A. Pines, *Angew. Chem. Int. Ed.* **2007**, *46*, 4064–4068; *Angew. Chem.* **2007**, *119*, 4142–4146; b) A. M. Balu, S. B. Duckett, R. Luque, *Dalton Trans.* **2009**, 5074–5076; c) K. V. Kovtunov, V. V. Zhivonitko, A. Corma, I. V. Koptyug, *J. Phys. Chem. Lett.* **2010**, *1*, 1705–1708; d) A. A. Lysova, I. V. Koptyug, *Chem. Soc. Rev.* **2010**, *39*, 4585–4601; e) I. V. Skovpin, V. V. Zhivonitko, I. V. Koptyug, *Appl. Magn. Res.* **2011**, *41*, 393–410; f) R. Zhou, E. W. Zhao, W. Cheng, L. M. Neal, H. Zheng, R. E. Quiñones, H. E. Hagelin-Weaver, C. R. Bowers, *J. Am. Chem. Soc.* **2015**, *137*, 1938–1946.

[7] a) P. Bhattacharya, E. Y. Chekmenev, W. F. Reynolds, S. Wagner, N. Zacharias, H. R. Chan, R. Buenger, B. D. Ross, *NMR Biomed.* **2011**, *24*, 1023–1028; b) P. Nikolaou, B. M. Goodson, E. Y. Chekmenev, *Chem. Eur. J.* **2015**, *21*, 3156–3166.

[8] a) S. B. Duckett, N. J. Wood, *Coord. Chem. Rev.* **2008**, *252*, 2278–2291; b) R. A. Green, R. W. Adams, S. B. Duckett, R. E. Mewis, D. C. Williamson, G. G. R. Green, *Prog. Nucl. Magn. Reson. Spectrosc.* **2012**, *67*, 1–48; c) S. B. Duckett, C. L. Newell, R. Eisenberg, *J. Am. Chem. Soc.* **1994**, *116*, 10548–10556.

[9] a) S. Abdulhussain, H. Breitzke, T. Ratajczyk, A. Gruenberg, M. Srour, D. Arnaut, H. Weidler, U. Kunz, H. J. Kleebe, U. Bommerich, J. Bernarding, T. Gutmann, G. Buntkowsky, *Chem. Eur. J.* **2014**, *20*, 1159–1166; b) C. Merckle, J. Blümel, *Top. Catal.* **2005**, *34*, 5–15; c) C. Merckle, S. Haubrich, J. Blümel, *J. Organomet. Chem.* **2001**, *627*, 44–54; d) R. H. Grubbs, L. C. Kroll, *J. Am. Chem. Soc.* **1971**, *93*, 3062–3063; e) J. Blümel, *Coord. Chem. Rev.* **2008**, *252*, 2410–2423; f) T. Gutmann, T. Ratajczyk, Y. Xu, H. Breitzke, A. Grünberg, S. Dillenberger, U. Bommerich, T. Trantzschel, J. Bernarding, G. Buntkowsky, *Solid State Nucl. Magn.* **2010**, *38*, 90–96; g) T. Gutmann, A. Grunberg, N. Rothermel, M. Werner, M. Srour, S. Abdulhussain, S. L. Tan, Y. P. Xu, H. Breitzke, G. Buntkowsky, *Solid State Nucl. Magn.* **2013**, *55–56*, 1–11; h) A. Grünberg, Y. P. Xu, H. Breitzke, G. Buntkowsky, *Chem. Eur. J.* **2010**, *16*, 6993–6998; i) L. Huang, J. C. Wu, S. Kawi, *React. Kinet. Catal. Lett.* **2004**, *82*, 65–71; j) I. V. Koptyug, K. V. Kovtunov, S. R. Burt, M. S. Anwar, C. Hilty, S.-I. Han, A. Pines, R. Z. Sagdeev, *J. Am. Chem. Soc.* **2007**, *129*, 5580–5586.

[10] a) J. R. Rapp, Y. Huang, M. Natella, Y. Cai, V. S. Y. Lin, M. Pruski, *Solid State Nucl. Magn.* **2009**, *35*, 82–86; b) S.-G. Shyu, S.-W. Cheng, D.-L. Tzou, *Chem. Commun.* **1999**, 2337–2338.

[11] E. Leitmannová, P. Jirasek, J. Rak, L. Potucka, P. Kacer, L. Cerveny, *Res. Chem. Intermed.* **2010**, *36*, 511–522.

[12] B. T. Heaton, J. A. Iggo, C. Jacob, J. Nadarajah, M. A. Fontaine, R. Messere, A. F. Noels, *J. Chem. Soc. Dalton Trans.* **1994**, 2875–2880.

[13] a) M. S. Sanford, J. A. Love, R. H. Grubbs, *Organometallics* **2001**, *20*, 5314–5318; b) J. A. Love, J. P. Morgan, T. M. Trnka, R. H. Grubbs, *Angew. Chem. Int. Ed.* **2002**, *41*, 4035–4037; *Angew. Chem.* **2002**, *114*, 4207–4209.

[14] T. Joseph, S. S. Deshpande, S. B. Halligudi, A. Vinu, S. Ernst, M. Hartmann, *J. Mol. Catal. A* **2003**, *206*, 13–21.

[15] F. Pardal, V. Lapinte, J. J. Robin, *J. Polym. Sci. Part A* **2009**, *47*, 4617–4628.

[16] B. J. van Rossum, H. Förster, H. J. M. de Groot, *J. Magn. Reson.* **1997**, *124*, 516–519.

[17] A. E. Bennett, C. M. Rienstra, M. Auger, K. V. Lakshmi, R. G. Griffin, *J. Chem. Phys.* **1995**, *103*, 6951–6958.

[18] a) J. Bargon in *The Handbook of Homogeneous Hydrogenation*, Wiley-VCH, **2008**, pp. 313–358; b) T. Gutmann, M. Sellin, H. Breitzke, A. Stark, G. Buntkowsky, *Phys. Chem. Chem. Phys.* **2009**, *11*, 9170–9175.

[19] M. G. Pravica, D. P. Weitekamp, *Chem. Phys. Lett.* **1988**, *145*, 255–258.

[20] a) G. Wu, R. E. Wasylishen, *Inorg. Chem.* **1996**, *35*, 3113–3116; b) J. W. Diesveld, E. M. Menger, H. T. Edzes, W. S. Veeman, *J. Am. Chem. Soc.* **1980**, *102*, 7935–7936; c) G. Wu, R. E. Wasylishen, *Organometallics* **1992**, *11*, 3242–3248.

[21] J. Bluemel, *Inorg. Chem.* **1994**, *33*, 5050–5056.

[22] J. Goodman, V. V. Grushin, R. B. Larichev, S. A. Macgregor, W. J. Marshall, D. C. Roe, *J. Am. Chem. Soc.* **2010**, *132*, 12013–12026.

[23] B. Hu, L. Delevoye, O. Lafon, J. Trébosc, J. Amoureux, *J. Magn. Reson.* **2009**, *200*, 178–188.

[24] K. V. Kovtunov, D. A. Barskiy, A. M. Coffey, M. L. Truong, O. G. Salnikov, A. K. Khudorozhkov, E. A. Inozemtseva, I. P. Prosvirin, V. I. Bukhtiyarov, K. W. Waddell, E. Y. Chekmenev, I. V. Koptyug, *Chem. Eur. J.* **2014**, *20*, 11636–11639.

Received: July 19, 2016
Published online on September 30, 2016